The Journal of Chemical Physics

RESEARCH ARTICLE | MARCH 25 2025

High-pressure and high-temperature thermoelasticity of tantalum: An *ab initio* study

Special Collection: Michele Parrinello Festschrift

X. Gong ; A. Dal Corso

J. Chem. Phys. 162, 124709 (2025)
https://doi.org/10.1063/5.0258989

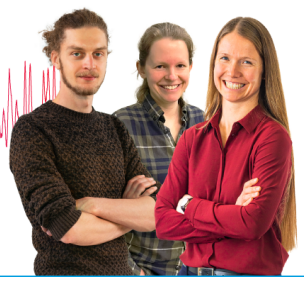

The Journal of Chemical Physics ARTICLE pubs.aip.org/aip/jcp

High-pressure and high-temperature thermoelasticity of tantalum: An *ab initio* study

Cite as: J. Chem. Phys. 162, 124709 (2025); doi: 10.1063/5.0258989
Submitted: 17 January 2025 • Accepted: 7 March 2025 •
Published Online: 25 March 2025

X. Gong[1,a] and A. Dal Corso[1,2]

AFFILIATIONS

[1] International School for Advanced Studies (SISSA), Via Bonomea 265, 34136 Trieste, Italy
[2] IOM—CNR, Via Bonomea 265, 34136 Trieste, Italy

Note: This paper is part of the JCP Special Topic, Michele Parrinello Festschrift.
[a] **Author to whom correspondence should be addressed:** xgong@sissa.it

ABSTRACT

We present the thermoelastic properties of the body-centered cubic tantalum calculated within the quasi-harmonic approximation (QHA) and compare them with those given by the quasi-static approximation (QSA) and those measured experimentally. We find that the QHA temperature dependent elastic constants (TDECs) follow the experiment very well from 5 K up to 500 K, and in this range of temperatures are in better agreement with the experiment than the QSA TDECs. At higher temperatures, our QHA results are linear with temperature and fail to follow the measured change in slope of $C(T)$ and $C_{44}(T)$ that become parallel to the QSA results. We also present our QHA pressure dependent elastic constants at 5, 300, 1000, and 1500 K.

I. INTRODUCTION

Tantalum, as a member of the refractory metals family (melting temperature T_M = 3269 K), is known for its high corrosion resistance and applications for electronics, environmental chemical processing, and medicine.[1] Tantalum is also a widely used component of metallic alloys. Its thermodynamic properties have been studied in detail, both experimentally[2–4] and *ab initio*.[5–9]

Temperature dependent elastic constants (TDECs) of tantalum present characteristic features such as a change of slope at high temperature[10,11] that have been the subject of extensive investigations. At room pressure, TDECs have been measured from 0 to 300 K in Refs. 12–14. The range from 300 to 725 K has been reported in Ref. 10, showing a linear dependence on temperature but with a somewhat different slope with respect to the values measured between 0 and 300 K. This change of slope has also been confirmed in Ref. 11, where the measurement has been extended from 300 K up to 3000 K. Pressure dependent elastic constants have been measured at room temperature in Refs. 15 and 16, but no experimental information is available for the high-temperature, high-pressure regime.

Pressure dependent elastic constants at 0 K calculated *ab initio*[17–19] are in reasonable agreement among themselves and with the available experiments. TDECs have been computed within the quasi-static approximation (QSA),[20,21] and there are claims that the QSA ECs can explain the anomalous temperature behavior found in the experiment,[21] in particular the minimum in the $C_{44}(T)$ curve. TDECs of tantalum within the quasi-harmonic approximation (QHA) have been computed in Ref. 22, but phonons were obtained with a model generalized pseudopotential theory (MGPT). In this case, reasonable agreement with the experiment has been found. Finally, QHA TDECs have been calculated within the PIC model,[23] but these calculations cover too large a range of temperatures and pressures to help the interpretation of the experimental data at room pressure.

In several metals,[24–27] we showed that the QHA is much more accurate than the QSA in predicting the TDECs at room pressure. QHA has also been found to be quite accurate in silicate minerals of geophysical interest (see, for instance, Ref. 28 and references therein) and in oxides such as MgO.[29,30] In this paper we present a comparison of the QSA and QHA TDECs of tantalum and use them to interpret the experimental data. Moreover, we present our

QHA prediction for the high temperature–high pressure regime. We include both the vibrational and the electronic excitation contributions in the free energy, and we find that, on a large scale, the QSA TDECs seem to be in better agreement with the experiment than the QHA ones. On a closer examination, however, the QHA accurately predicts the temperature variation of the combination of elastic constants measured in experiments from 0 to ~500 K, but then fails to predict the change of slope found in experiments at higher temperatures. Our QHA ECs do not present any anomalous behavior: they decrease linearly with temperature at the same slope observed until 500 K. These results may point to the existence of relevant effects not accounted for by the QHA, such as the anharmonic phonon–phonon interactions.

For completeness, the phonon dispersions and the thermodynamic properties already available in the literature, such as the thermal equation of state, thermal expansion, isobaric heat capacity, and adiabatic bulk modulus calculated by density functional theory using the local density approximation (LDA),[31] the PBE,[32] and the PBEsol[33] generalized gradient approximations, are presented in the supplementary material.

II. THEORY AND COMPUTATIONAL DETAILS

The QHA, as implemented in the `thermo_pw` software, has been discussed in previous publications.[24–26,34–38] We refer to these papers for the theory used in the present work. Here, we remind only that within the QHA, the Helmholtz free energy of a solid is a function of temperature T and of the strain ε_{ij}. It can be written as the sum of three contributions,

$$F(\varepsilon_{ij}, T) = U(\varepsilon_{ij}) + F_{ph}(\varepsilon_{ij}, T) + F_{el}(\varepsilon_{ij}, T), \tag{1}$$

where $U(\varepsilon_{ij})$ is the static energy, computed via density functional theory (DFT), $F_{ph}(\varepsilon_{ij}, T)$ is the vibrational free energy written in terms of the phonon frequencies $\omega_\eta(\mathbf{q}, \varepsilon_{ij})$, and $F_{el}(\varepsilon_{ij}, T)$ is the electronic free energy computed within the rigid bands approximation from the electronic density of states (see Ref. 25).

The isothermal QHA ECs are calculated from the second strain derivatives of the free energy

$$\tilde{C}^T_{ijkl} = \frac{1}{V}\frac{\partial^2 F}{\partial\varepsilon_{ij}\partial\varepsilon_{kl}}\bigg|_T, \tag{2}$$

correcting, at finite pressure, to obtain the stress–strain ECs,[39]

$$C^T_{ijkl} = \tilde{C}^T_{ijkl} + \frac{p}{2}\left(2\delta_{i,j}\delta_{k,l} - \delta_{i,l}\delta_{j,k} - \delta_{i,k}\delta_{j,l}\right). \tag{3}$$

The second derivatives of the free energy are calculated as described in Ref. 24, taking a subset of the volumes V_i (used for computing the thermal expansion) as equilibrium configurations. The ECs at any other volume at temperature T and pressure p are obtained by interpolation by a fourth-degree polynomial. Adiabatic ECs are calculated from the isothermal ones as

$$C^S_{ijkl} = C^T_{ijkl} + \frac{TVb_{ij}b_{kl}}{C_V}, \tag{4}$$

where b_{ij} are the thermal stresses

$$b_{ij} = -\sum_{kl} C^T_{ijkl}\alpha_{kl}, \tag{5}$$

and C_V is the isochoric heat capacity (see C_P in the supplementary material). For a cubic system, the linear thermal expansion tensor is diagonal, and from the volume thermal expansion β_V, we obtain $\alpha_{kl} = \delta_{kl}\beta_V/3$.

The calculations presented in this work are performed by using DFT as implemented in the Quantum ESPRESSO package.[40,41] The exchange and correlation functionals that we have considered are the LDA[31] and the generalized gradient approximations PBEsol[33] and PBE.[32] TDECs have been calculated only with the PBE functional.

We employ the projector augmented wave (PAW) method[42] and a plane-wave basis with pseudopotentials from `pslibrary`.[43] We use `Ta.pz-spn-kjpaw_psl.1.0.0.UPF`, `Ta.pbesol-spn-kjpaw_psl.1.0.0.UPF`, and `Ta.pbe-spn-kjpaw_psl.1.0.0.UPF` for LDA, PBEsol, and PBE, respectively. These pseudopotentials have the 5*s*, 5*p*, 5*d*, and 6*s* states in the valence, while the other states are frozen in the core and accounted for by the nonlinear core correction.[44] For the wave function cutoffs, we use 70 Ry, 80 Ry, and 90 Ry, while for the charge density we use 280 Ry, 320 Ry, and 360 Ry for LDA, PBEsol, and PBE, respectively. The Fermi surface has been dealt with by a smearing approach[45] with a smearing parameter $\sigma = 0.02$ Ry. With this smearing, the Brillouin zone integrals converge with a $40 \times 40 \times 40$ **k**-point mesh.

Density functional perturbation theory (DFPT)[46,47] is used to calculate the dynamical matrices on a $10 \times 10 \times 10$ **q**-point grid. These dynamical matrices have been Fourier interpolated on a $200 \times 200 \times 200$ **q**-point mesh to evaluate the free-energy and the thermodynamic quantities.

The harmonic and quasi-harmonic thermodynamic quantities are calculated by the `thermo_pw` code.[48] For quasi-harmonic calculations, the free energy and, therefore, the electronic density of states and the phonon dispersions are calculated in $N_V = 17$ geometries with lattice constants from $a_0 - 1.2$ a.u. to $a_0 + 0.4$ a.u. in steps of $\Delta a = 0.1$ a.u., where a_0 is the equilibrium 0 K lattice constant (see Table I).

QHA TDECs have been calculated on six geometries from $N_i = 9$ to $N_i = 14$. TDECs at higher pressures could not be computed for the presence of imaginary frequencies in some distorted configurations. At geometry $N_i = 9$, the pressure is about 700 kbar, so QHA ECs should be reliable in the range of pressures presented here.

All calculations have been performed on the Leonardo supercomputer at CINECA with a GPU optimized version of `thermo_pw`.[49]

III. RESULTS AND DISCUSSION

We report in Table I the equilibrium lattice constants, bulk moduli, and pressure derivatives of the bulk moduli obtained as parameters of a fourth-order Birch–Murnaghan interpolation of the static energy and compare them with a few selected values from previous calculations and experiments. In order to estimate the thermal effects, we also report the parameters obtained by interpolating the Helmholtz free energy at 295 K. Taking the all-electron calculation of the lattice constants of Ref. 50 as reference, our PAW values are smaller than 0.2% with all functionals. With respect to the experiment of Ref. 4, corrected for zero point and temperature effects by subtracting 0.013 a.u. that gives 6.232 a.u., the errors of LDA, PBEsol, and PBE are −1.3%, −0.6%, and 0.5%, respectively. Taking

TABLE I. Equilibrium lattice constants (a_0), the bulk moduli (B_T), and the pressure derivatives of the bulk moduli (B'_T) of tantalum calculated in this work compared with previous calculations and with experimental data (in the experiment, B_S is measured at 300 K. At 0 K, B_S and B_T have the same value).

		T (K)	a_0 (a.u.)	B_T (kbar)	B'_T
This study	LDA	0	6.140	2165	3.51
		295	6.152	2100	3.70
	PBEsol	0	6.192	2072	3.47
		295	6.205	2007	3.64
	PBE	0	6.264	1948	3.53
		295	6.277	1902	3.60
Calc.[50]	LDA	0	6.155		
	PBEsol	0	6.208		
	PBE	0	6.280		
Calc.[23]	PBE	0	6.100		
Calc.[5]	PBE	0	6.293	1944	3.06
Expt.[4]		300	6.245	1947	3.4
Expt.[12]		0		1942	
		300	6.247	1919	
Expt.[13]		0		1964	
		300		1939	

as the experimental value of the bulk modulus 1942 kbar reported by Ref. 12, the errors of LDA, PBEsol, and PBE are 11%, 7%, and 0.3%. All functionals overestimate the bulk modulus, but PBE is quite close to the experimental value.

In Table II, we report the calculated elastic constants at the equilibrium 0 K lattice constant. Assuming as 0 K experimental values C_{11} = 2663 kbar, C_{12} = 1582 kbar, and C_{44} = 874 kbar of Ref. 12, the LDA errors are 358 kbar (13%), 161 kbar (10%), and −164 kbar (−19%); the PBEsol errors are 199 kbar (7%), 91 kbar (6%), and −119 kbar (−14%); while the PBE errors are −16 kbar (−0.6%), 13 kbar (0.8%), and −134 kbar (−15%). With the exception of C_{44}, for which the three functionals have similar errors, the PBE functional is the closest to the experimental values.

As we have shown in a previous paper,[26] the temperature dependence of the ECs is not strongly influenced by the exchange and correlation functional that instead can change the 0 K values. Therefore, in the following, we limit the calculations of the TDECs, which are numerically heavy, to the PBE functional.

After computing the PBE TDECs, we can estimate the zero point motion (ZPM) effects on the elastic constants for this functional. The effect is not large but not totally negligible, as shown in Table II and as already pointed out in the literature for other systems with lighter atoms.[28] Assuming the same change also for the other functionals, the LDA errors become 311 kbar (12%), 133 kbar (8%), and −179 kbar (−20%); the PBEsol errors become 152 kbar (6%), 63 kbar (4%), and −134 kbar (−15%); while the PBE errors become −63 kbar (−2%), −15 kbar (−0.9%), and −149 kbar (−17%). In Table II, we report, for comparison, the 300 K values of the adiabatic elastic constants as well. At this temperature the thermal decreases are comparable to those due to ZPM.

In Fig. 1, we report the 0 K ECs calculated as a function of pressure. At room pressure we find $\frac{dC_{11}}{dp}$ = 4.9, $\frac{dC_{12}}{dp}$ = 3.1, and $\frac{dC_{44}}{dp}$ = 1.0 to be compared with the experimental values $\frac{dC_{11}}{dp}$ = 5.1, $\frac{dC_{12}}{dp}$ = 3.14, and $\frac{dC_{44}}{dp}$ = 0.995 from Ref. 16. Our data are in good agreement with Ref. 17. C_{11} and C_{12} are also in good agreement with Ref. 19, while our C_{44} value is above this reference.

In Fig. 2, we compare the QSA adiabatic TDECs with the experiment and with the previous PBE calculation of Ref. 20. The two calculations are in substantial agreement, with slightly different values of the 0 K ECs. On the scale of this figure, the QSA ECs follow well the experimental results of Ref. 10 and Ref. 11 since the QSA TDECs have a slope that agrees with the high temperature slope of the tantalum ECs. Passing from 5 to 2000 K, the decrease is

TABLE II. Elastic constants calculated with the different functionals compared with the experiment and two previous calculations. B, E, G, and ν are the bulk modulus, the Young's modulus, the shear modulus, and the Poisson's ratio, respectively. ZPM indicates that zero point motion effects have been included.

	T (K)	a_0 (a.u.)	C_{11} (kbar)	C_{12} (kbar)	C_{44} (kbar)	B (kbar)	E (kbar)	G (kbar)	ν
LDA	0	6.138	3021	1743	710	2169	1849	681	0.358
PBEsol	0	6.189	2862	1673	755	2069	1853	686	0.351
PBE	0	6.262	2647	1595	740	1946	1743	645	0.351
PBE	0 + ZPM	6.268	2600	1567	725	1911	1710	633	0.351
PBE	300	6.278	2540	1548	674	1878	1617	596	0.357
PBE[17]	0	6.253	2650	1590	740	1943	1748	647	0.350
GGA[19]	0	6.357	2636	1600	514	1945	1421	515	0.378
Expt.[12]	0		2663	1582	874	1942	1924	721	0.335
Expt.[13]	0		2701	1595	873	1964	1941	727	0.335
Expt.[11]	0		2665	1582	873	1943	1924	721	0.335
Expt.[12]	300		2609	1574	818	1919	1826	680	0.341
Expt.[10]	300		2602	1544	826	1897	1848	691	0.338
Expt.[16]	300		2661	1610	824	1960	1847	688	0.343
Expt.[15]	300		2536	1627	719	1930	1627	598	0.359

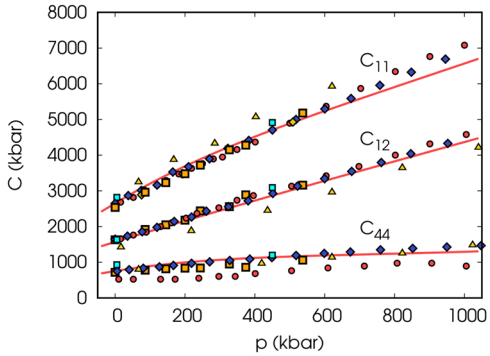

FIG. 1. $T = 0$ K elastic constants C_{11}, C_{12}, and C_{44} as a function of pressure calculated within PBE compared with the experiment[15] (orange squares). As a reference, we also report previous calculations of the PBE results of Ref. 17 (blue diamonds), Ref. 19 (red circles), Ref. 18 (yellow triangles), and Ref. 51 (cyan squares).

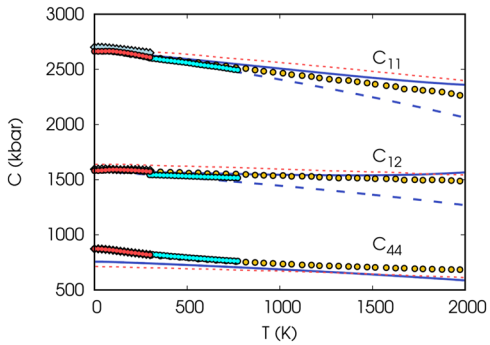

FIG. 2. Comparison of the PBE adiabatic QSA elastic constants C_{11}, C_{12}, and C_{44} (continuous blue line) as a function of temperature with experiments from Ref. 12 (red dots), Ref. 11 (yellow dots), Ref. 13 (light blue diamonds), and Ref. 10 (cyan dots). Dashed lines indicate the isothermal elastic constants. The dotted red line is the PBE QSA calculation of Ref. 20.

$\Delta C_{11} = 298$ kbar (11%), $\Delta C_{12} = 7$ kbar (0.4%), and $\Delta C_{44} = 169$ kbar (22%), compared to the experimental values from Ref. 11: $\Delta C_{11} = 408$ kbar (15%), $\Delta C_{12} = 102$ kbar (6%), and $\Delta C_{44} = 188$ kbar (22%). For comparison, we also report the calculated isothermal ECs, which decrease more rapidly than the adiabatic ones since the correction term due to thermal stresses in Eq. (4) is positive.

The QHA adiabatic ECs are shown in Fig. 3 and compared with the experimental results. The QHA ECs decrease with temperature more than the QSA ones. Passing from 5 to 2000 K, we have $\Delta C_{11} = 595$ kbar (22%), $\Delta C_{12} = 260$ kbar (16%), and $\Delta C_{44} = 423$ kbar (57%). Therefore, in this extended temperature range, the QSA ECs are in better agreement with the experiments than the QHA ECs.

A comparison of the QSA and QHA TDECs is presented in Fig. 4. In this figure, we have limited the temperature from 0 to 1200 K, a range where the QHA is expected to be a good approximation. The difference between the two approximations is not large, but still the QHA seems to worsen the agreement with

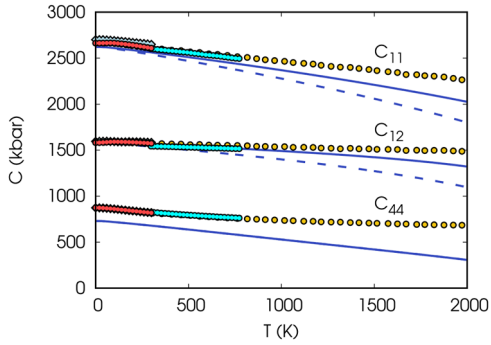

FIG. 3. Comparison of the PBE adiabatic QHA elastic constants C_{11}, C_{12}, and C_{44} (continuous blue line) as a function of temperature with experiments from Ref. 12 (red dots), Ref. 11 (yellow dots), Ref. 13 (light blue diamonds), and Ref. 10 (cyan dots). Dashed lines indicate the isothermal elastic constants.

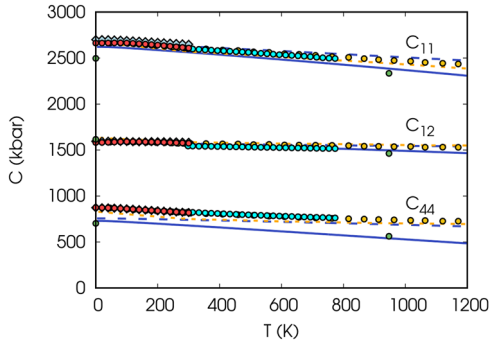

FIG. 4. Comparison of the PBE QSA (dashed blue line) and QHA (solid blue line) elastic constants C_{11}, C_{12}, and C_{44} as a function of temperature. The experiments are from Ref. 12 (red dots), Ref. 11 (yellow dots), Ref. 13 (light blue diamonds), and Ref. 10 (cyan dots). The green dots represent the PBE results of Ref. 23. The dashed orange line is the calculation of Ref. 22.

the experiment. For comparison, we also report the QHA calculation of Ref. 22. These data follow our QSA calculation better than the QHA one.

In order to better interpret the results, we present in Figs. 5–7 the combination of elastic constants $C = \frac{1}{2}(C_{11} + C_{12} + 2C_{44})$, $C' = \frac{1}{2}(C_{11} - C_{12})$, and C_{44} after subtracting their 0 K value. These combinations are measured in the experiment, while the elastic constants themselves are derived from them. We plot both the QSA and the QHA results. The QHA C and C_{44} closely follow the experimental data from 0 K to about 500 K but fail to predict the change in slope measured in the experiment at higher temperatures. QHA C', on the other hand, is in agreement with the experiment across the entire temperature range, while QSA C' is higher. In these figures, we also report the QSA results from Ref. 21, which are in good agreement with our QSA results. In the supplementary material, we report similar pictures for $C_{11} = C + C' - C_{44}$ and $C_{12} = C - C' - C_{44}$. At low temperatures, these curves are more challenging to interpret, and the situation remains unclear, while at higher temperatures, the slope continues to align with that predicted by QSA, as already illustrated in Fig. 4.

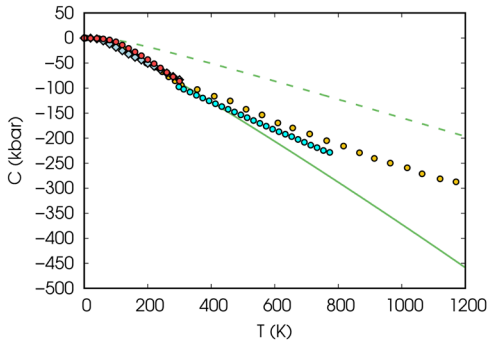

FIG. 5. PBE adiabatic QSA (dashed line) and QHA (continuous line) combinations of elastic constants $C = 0.5(C_{11} + C_{12} + 2C_{44})$ as a function of temperature after subtracting the $T = 0$ K value. The function is compared with experiments from Ref. 12 (red dots), Ref. 11 (yellow dots), Ref. 13 (light blue diamonds), and Ref. 10 (cyan dots).

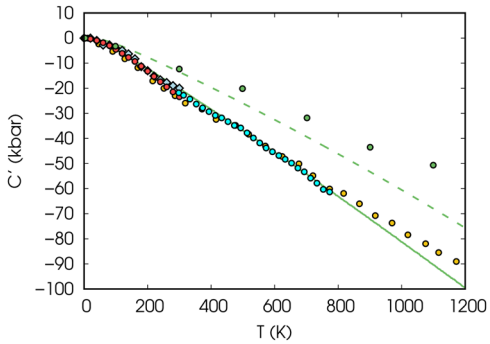

FIG. 6. PBE adiabatic QSA (dashed line) and QHA (continuous line) combinations of elastic constants $C' = 0.5(C_{11} - C_{12})$ as a function of temperature after subtracting the $T = 0$ K value. The function is compared with experiments from Ref. 12 (red dots), Ref. 11 (yellow dots), Ref. 13 (light blue diamonds), and Ref. 10 (cyan dots). The QSA results of Ref. 21 are also shown (green dots).

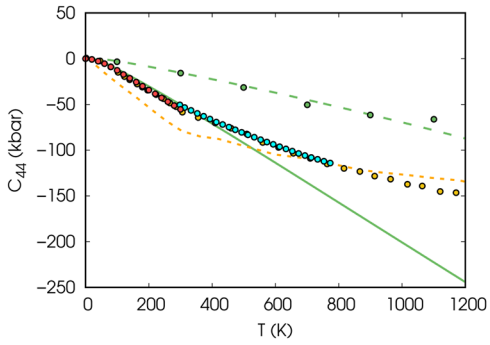

FIG. 7. PBE adiabatic QSA (dashed line) and QHA (continuous line) C_{44} elastic constants as a function of temperature after subtracting the $T = 0$ K value. Theory is compared with experiments from Ref. 12 (red dots), Ref. 11 (yellow dots), Ref. 13 (light blue diamonds), and Ref. 10 (cyan dots). The QSA results of Ref. 21 are also shown (green dots). The orange dashed line shows the results of Ref. 22.

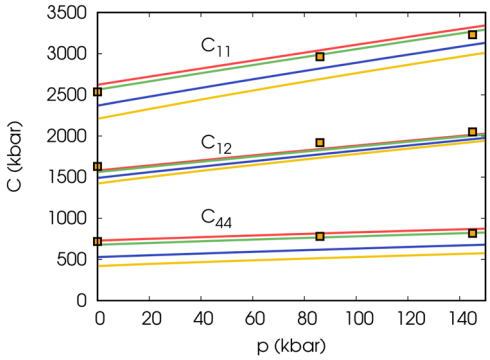

FIG. 8. QHA adiabatic elastic constants C_{11}, C_{12}, and C_{44} as a function of pressure calculated within PBE at 5 K (red line), 300 K (green line), 1000 K (blue line), and 1500 K (yellow line). The orange squares represent the experimental data of Ref. 15 measured at room temperature.

Finally, we present in Fig. 8 the adiabatic QHA elastic constants as a function of pressure at different temperatures: 5, 300, 1000, and 1500 K. Except for the room temperature data from Ref. 15, which are in reasonable agreement with our calculations, we have not found any other experimental data at higher temperatures to compare with our results.

IV. CONCLUSIONS

We presented the QHA TDECs of tantalum calculated within the PBE exchange and correlation functional, and we compared them with the QSA TDECs. QHA gives a better agreement with the experiment than QSA at low temperatures, up to 500 K, for the quantities C, C', and C_{44} that are measured in experiments. At high temperatures, experiments show a change of slope of the temperature dependent curves that is not reproduced by our calculations. When comparing C_{11} and C_{12}, the situation is less clear at low temperatures, and across a large temperature range from 0 to 2000 K, the QSA TDECs appear closer to experimental results than the QHA ones. None of the two approximations, however, predict the change of slope measured in experiments.

We also presented the pressure dependent QHA elastic constants both at 5, 300, 1000, and 1500 K that could be compared with the experiment only at 300 K. We hope that these data will stimulate a measurement of the tantalum ECs at high temperature and pressure, a piece of information still missing from the literature.

SUPPLEMENTARY MATERIAL

The supplementary material contains the calculated phonon dispersions, the thermal equation of state, thermodynamic properties already available in the literature, and additional elastic constants plots.

ACKNOWLEDGMENTS

This work was supported by the Italian MUR (Ministry of University and Research) through the National Center for HPC, Big Data, and Quantum Computing (Grant No. CN00000013). Computational facilities were provided by SISSA through its Linux Cluster, ITCS, and the SISSA-CINECA 2021–2024 Agreement. Partial support was received from MAX "MAterials design at the eXascale" Center of Excellence for Supercomputing Applications (Grant Agreement No. 101093374, co-funded by the European High Performance Computing Joint Undertaking (JU) of the European Union and participating countries).

AUTHOR DECLARATIONS

Conflict of Interest

The authors have no conflicts to disclose.

Author Contributions

X. Gong: Conceptualization (equal); Data curation (equal); Formal analysis (equal); Investigation (equal); Methodology (equal); Software (equal); Validation (equal); Visualization (equal); Writing – original draft (equal); Writing – review & editing (equal). **A. Dal Corso**: Conceptualization (equal); Data curation (equal); Formal analysis (equal); Funding acquisition (equal); Investigation (equal); Methodology (equal); Project administration (equal); Resources (equal); Software (equal); Supervision (equal); Validation (equal); Visualization (equal); Writing – original draft (equal); Writing – review & editing (equal).

DATA AVAILABILITY

The data that support the findings of this study are available from the corresponding author upon reasonable request.

REFERENCES

[1] S. M. Cardonne, P. Kumar, C. A. Michaluk, and H. D. Schwartz, "Tantalum and its alloys," Int. J. Refract. Met. Hard Mater. **13**, 187–194 (1995).
[2] J. W. Arblaster, "Thermodynamic properties of tantalum," J. Phase Equilib. Diffus. **39**, 255–272 (2018).
[3] A. Dewaele, P. Loubeyre, and M. Mezouar, "Equations of state of six metals above 94 GPa," Phys. Rev. B **70**, 094112 (2004).
[4] H. Cynn and C.-S. Yoo, "Equation of state of tantalum to 174 GPa," Phys. Rev. B **59**, 8526–8529 (1999).
[5] Z.-L. Liu, L.-C. Cai, X.-R. Chen, Q. Wu, and F.-Q. Jing, "*Ab initio* refinement of the thermal equation of state for bcc tantalum: The effect of bonding on anharmonicity," J. Phys.: Condens. Matter **21**, 095408 (2009).
[6] M. Foata-Prestavoine, G. Robert, M.-H. Nadal, and S. Bernard, "First-principles study of the relations between the elastic constants, phonon dispersion curves, and melting temperatures of bcc Ta at pressures up to 1000 GPa," Phys. Rev. B **76**, 104104 (2007).
[7] S. Taioli, C. Cazorla, M. J. Gillan, and D. Alfè, "Melting curve of tantalum from first principles," Phys. Rev. B **75**, 214103 (2007).
[8] C. Bercegeay and S. Bernard, "First-principles equations of state and elastic properties of seven metals," Phys. Rev. B **72**, 214101 (2005).
[9] R. E. Cohen and O. Gülseren, "Thermal equation of state of tantalum," Phys. Rev. B **63**, 224101 (2001).
[10] N. Soga, "Comparison of measured and predicted bulk moduli of tantalum and tungsten at high temperatures," J. Appl. Phys. **37**, 3416–3420 (1966).
[11] E. Walker and P. Bujard, "Anomalous temperature behaviour of the shear elastic constant C_{44} in tantalum," Solid State Commun. **34**, 691–693 (1980).
[12] F. H. Featherston and J. R. Neighbours, "Elastic constants of tantalum, tungsten, and molybdenum," Phys. Rev. **130**, 1324–1333 (1963).
[13] R. G. Leisure, D. K. Hsu, and B. A. Seiber, "Elastic properties of tantalum over the temperature range 4–300 K," J. Appl. Phys. **44**, 3394–3397 (1973).
[14] C. E. Anderson and F. R. Brotzen, "Elastic constants of tantalum-tungsten alloys," J. Appl. Phys. **53**, 292–297 (1982).
[15] H. Fukui, A. Yoneda, S. Kamada, H. Uchiyama, N. Hirao, and A. Q. R. Baron, "Single crystal elasticity and equation of state of tantalum up to 54 GPa," J. Appl. Phys. **132**, 055902 (2022).
[16] K. W. Katahara, M. H. Manghnani, and E. S. Fisher, "Pressure derivatives of the elastic moduli of niobium and tantalum," J. Appl. Phys. **47**, 434–439 (1976).
[17] L. Koči, Y. Ma, A. R. Oganov, P. Souvatzis, and R. Ahuja, "Elasticity of the superconducting metals V, Nb, Ta, Mo, and W at high pressure," Phys. Rev. B **77**, 214101 (2008).
[18] J.-B. Gu, C.-J. Wang *et al.*, "High-pressure structure and elastic properties of tantalum single crystal: First principles investigation," Chin. Phys. B **25**, 126103 (2016).
[19] X. Qi, S. Wang, S. Chen, N. Cai, and B. Li, "Anomalous elastic behavior of tantalum at high pressures: Experimental and theoretical studies," Int. J. Refract. Met. Hard Mater. **101**, 105691 (2021).
[20] Y. Wang, J. J. Wang, H. Zhang, V. R. Manga, S. L. Shang, L.-Q. Chen, and Z.-K. Liu, J. Phys.: Condens. Matter **22**, 225404 (2010).
[21] P. Keuter, D. Music, V. Schnabel, M. Stuer, and J. M. Schneider, "From qualitative to quantitative description of the anomalous thermoelastic behavior of V, Nb, Ta, Pd and Pt," J. Phys.: Condens. Matter **31**, 225402 (2019).
[22] D. Orlikowski, P. Söderlind, and J. A. Moriarty, "First-principles thermoelasticity of transition metals at high pressure: Tantalum prototype in the quasiharmonic limit," Phys. Rev. B **74**, 054109 (2006).
[23] O. Gülseren and R. E. Cohen, "High-pressure thermoelasticity of body-centered-cubic tantalum," Phys. Rev. B **65**, 064103 (2002).
[24] C. Malica and A. D. Corso, "Quasi-harmonic temperature dependent elastic constants: Applications to silicon, aluminum, and silver," J. Phys.: Condens. Matter **32**, 315902 (2020).
[25] C. Malica and A. Dal Corso, "Quasi-harmonic thermoelasticity of palladium, platinum, copper, and gold from first principles," J. Phys.: Condens. Matter **33**, 475901 (2021).
[26] X. Gong and A. Dal Corso, "Pressure and temperature dependent ab-initio quasi-harmonic thermoelastic properties of tungsten," J. Phys.: Condens. Matter **36**, 285702 (2024).
[27] X. Gong and A. Dal Corso, "*Ab initio* quasi-harmonic thermoelasticity of molybdenum at high temperature and pressure," J. Chem. Phys. **160**, 244703 (2024).
[28] C. Luo, X. Deng, W. Wang, G. Shukla, Z. Wu, and R. M. Wentzcovitch, "cij: A python code for quasiharmonic thermoelasticity," Comput. Phys. Commun. **267**, 108067 (2021).
[29] Z. Wu and R. M. Wentzcovitch, "Quasiharmonic thermal elasticity of crystals: An analytical approach," Phys. Rev. B **83**, 184115 (2011).
[30] F. Zou, Z. Wu, W. Wang, and R. M. Wentzcovitch, "An extended semianalytical approach for thermoelasticity of monoclinic crystals: Application to diopside," J. Geophys. Res.: Solid Earth **123**, 7629–7643, https://doi.org/10.1029/2018jb016102 (2018).
[31] J. P. Perdew and A. Zunger, "Self-interaction correction to density-functional approximations for many-electron systems," Phys. Rev. B **23**, 5048–5079 (1981).
[32] J. P. Perdew, K. Burke, and M. Ernzerhof, "Generalized gradient approximation made simple," Phys. Rev. Lett. **77**, 3865–3868 (1996).
[33] J. P. Perdew, A. Ruzsinszky, G. I. Csonka, O. A. Vydrov, G. E. Scuseria, L. A. Constantin, X. Zhou, and K. Burke, "Restoring the density-gradient expansion for exchange in solids and surfaces," Phys. Rev. Lett. **100**, 136406 (2008).
[34] A. Dal Corso, "Elastic constants of beryllium: A first-principles investigation," J. Phys.: Condens. Matter **28**, 075401 (2016).

[35]M. Palumbo and A. Dal Corso, "Lattice dynamics and thermophysical properties of h.c.p. Os and Ru from the quasi-harmonic approximation," J. Phys.: Condens. Matter **29**, 395401 (2017).
[36]M. Palumbo and A. Dal Corso, "Lattice dynamics and thermophysical properties of h.c.p. Re and Tc from the quasi-harmonic approximation," Phys. Status Solidi B **254**, 1700101 (2017).
[37]C. Malica and A. Dal Corso, "Temperature-dependent atomic B factor: An *ab initio* calculation," Acta Crystallogr., Sect. A: Found. Adv. **75**, 624–632 (2019).
[38]C. Malica and A. Dal Corso, "Temperature dependent elastic constants and thermodynamic properties of BAs: An *ab initio* investigation," J. Appl. Phys. **127**, 245103 (2020).
[39]T. H. K. Barron and M. L. Klein, "Second-order elastic constants of a solid under stress," Proc. Phys. Soc. **85**, 523 (1965).
[40]P. Giannozzi, S. Baroni, N. Bonini, M. Calandra, R. Car, C. Cavazzoni, D. Ceresoli, G. L. Chiarotti, M. Cococcioni, I. Dabo, A. Dal Corso, S. de Gironcoli, S. Fabris, G. Fratesi, R. Gebauer, U. Gerstmann, C. Gougoussis, A. Kokalj, M. Lazzeri, L. Martin-Samos, N. Marzari, F. Mauri, R. Mazzarello, S. Paolini, A. Pasquarello, L. Paulatto, C. Sbraccia, S. Scandolo, G. Sclauzero, A. P. Seitsonen, A. Smogunov, P. Umari, and R. M. Wentzcovitch, "QUANTUM ESPRESSO: A modular and open-source software project for quantum simulations of materials," J. Phys.: Condens. Matter **21**, 395502 (2009).
[41]P. Giannozzi, O. Andreussi, T. Brumme, O. Bunau, M. Buongiorno Nardelli, M. Calandra, R. Car, C. Cavazzoni, D. Ceresoli, M. Cococcioni, N. Colonna, I. Carnimeo, A. Dal Corso, S. de Gironcoli, P. Delugas, R. A. DiStasio, A. Ferretti, A. Floris, G. Fratesi, G. Fugallo, R. Gebauer, U. Gerstmann, F. Giustino, T. Gorni, J. Jia, M. Kawamura, H.-Y. Ko, A. Kokalj, E. Küçükbenli, M. Lazzeri, M. Marsili, N. Marzari, F. Mauri, N. L. Nguyen, H.-V. Nguyen, A. Otero-de-la Roza, L. Paulatto, S. Poncé, D. Rocca, R. Sabatini, B. Santra, M. Schlipf, A. P. Seitsonen, A. Smogunov, I. Timrov, T. Thonhauser, P. Umari, N. Vast, X. Wu, and S. Baroni, "Advanced capabilities for materials modelling with Quantum ESPRESSO," J. Phys.: Condens. Matter **29**, 465901 (2017).
[42]P. E. Blöchl, "Projector augmented-wave method," Phys. Rev. B **50**, 17953–17979 (1994).
[43]pslibrary can be found at the webpage, 2010, see https://github.com/dalcorso/pslibrary.
[44]S. G. Louie, S. Froyen, and M. L. Cohen, "Nonlinear ionic pseudopotentials in spin-density-functional calculations," Phys. Rev. B **26**, 1738–1742 (1982).
[45]M. Methfessel and A. T. Paxton, "High-precision sampling for Brillouin-zone integration in metals," Phys. Rev. B **40**, 3616–3621 (1989).
[46]S. Baroni, S. de Gironcoli, A. Dal Corso, and P. Giannozzi, "Phonons and related crystal properties from density-functional perturbation theory," Rev. Mod. Phys. **73**, 515–562 (2001).
[47]A. Dal Corso, "Density functional perturbation theory within the projector augmented wave method," Phys. Rev. B **81**, 075123 (2010).
[48]THERMO_pw can be found at the webpage, 2014, see https://github.com/dalcorso/thermo_pw.
[49]X. Gong and A. Dal Corso, "An alternative GPU acceleration for a pseudopotential plane-waves density functional theory code with applications to metallic systems," Comput. Phys. Commun. **308**, 109439 (2025).
[50]P. Haas, F. Tran, and P. Blaha, "Calculation of the lattice constant of solids with semilocal functionals," Phys. Rev. B **79**, 085104 (2009).
[51]P. Söderlind and J. A. Moriarty, "First-principles theory of Ta up to 10 Mbar pressure: Structural and mechanical properties," Phys. Rev. B **57**, 10340–10350 (1998).